

Design and Simulation of an Orbiting Piezoelectric MEMS Gyroscope Based on Phase-Shift Signals

Sergey Gorelick^{*1}

¹VTT Technical Research Centre of Finland, Tietotie 3, Espoo, P.O.Box 1000, FI-02044 VTT, Finland

*Corresponding author: Tietotie 3, Espoo, P.O.Box 1000, FI-02044 VTT, Finland; sergey.gorelick@vtt.fi

Abstract: By driving identical and orthogonal modes of a mass-on-springs system into resonance with harmonic excitations having $\pi/2$ rad phase difference, orbiting motion of the proof mass can be achieved. External rotation of the system modifies its mechanical response manifested in a phase-shift at resonance that is nearly proportional to the angular rates. In this study, the feasibility of phase-sensitive detection of angular rates using orbiting resonators suspended by thick annular springs with thin-film aluminium nitride piezoactuators on top of the springs was investigated using simulations. The performance of the piezoresonators was simulated in a one-port drive-sense configuration in frequency domain and accounting for the action of the Coriolis force on the proof mass. The high sensitivities of the orbiting piezogyroscopes to the angular rates were obtained from the phase-shift at the resonance frequency of the motional current.

Keywords: MEMS gyroscope, piezoactuation, annular spring, ring-shaped spring, aluminium nitride

1. Introduction

MEMS vibratory gyroscopes are based on excitation of a primary vibration mode of a mass on springs, and detection of the mass motion due to the Coriolis force in the direction orthogonal to the primary mode. A novel approach is to drive both orthogonal modes simultaneously [1]. The general equation of motion of such a two degrees of freedom system of a common mass, m , on springs can be written as follows:

$$\begin{aligned} \ddot{x} + \frac{\omega_x}{Q_x} \dot{x} + \omega_x^2 x &= \frac{F_x}{m} e^{i\omega t} + 2\Omega \dot{y} \\ \ddot{y} + \frac{\omega_y}{Q_y} \dot{y} + \omega_y^2 y &= \frac{F_y}{m} e^{i(\omega t + \phi)} - 2\Omega \dot{x} \end{aligned} \quad (1)$$

where $\omega_{x,y} = 2\pi f_{x,y}$ are the resonance frequencies, $Q_{x,y}$ - quality factors, $F_{x,y}$ - driving force amplitudes of the orthogonal X and Y modes, respectively; Ω - angular rate about the

Z -axis and ϕ - phase difference between the X - and Y -driving forces. For identical orthogonal X - and Y -modes ($\omega_{x,y} = \omega_0$, $Q_{x,y} = Q$) driving modes into resonance with identical harmonic excitations, $F_{x,y} = F_0$, having $\phi = \pi/2$ rad phase difference results in the proof mass, m , performing a motion along a circular path about its centre of mass. It can be shown that in such an orbiting system the external rotation Ω modifies its mechanical response which is manifested as a phase-shift of the amplitude at resonance $\varphi = \tan^{-1} \frac{-\omega_0^2}{2Q\Omega}$. For low quality factors Q and values of Ω the phase-shift φ is nearly proportional to the angular rates. The system, therefore, can operate as a phase-sensitive gyroscope with potentially greater sensitivity and simplified read-out electronics compared to conventional MEMS gyroscopes relying on amplitude-signals.

In this paper the feasibility of phase-sensitive detection of angular rates using an orbiting mass suspended by annular springs with thin-film aluminium nitride (AlN) piezoactuators processed directly on top of them (Fig. 1) was investigated using Piezoelectric Devices interface of COMSOL MultiphysicsTM. The use of simulations allows studying more complex behaviours of the system not easily treatable analytically, e.g., response to the angular rates of the system having a mismatch between the resonance frequencies of the orthogonal modes, effect of the mode-coupling, effect of the structural non-idealities leading for non-symmetric driving/sensing between the modes, as well as verifying various driving and read-out schemes. The results of this study are important for understanding the design trade-offs in the phase-sensitive orbiting piezo-gyroscope.

2. Design of orbiting resonators

The decoupling of the orthogonal resonance modes is important for the optimal performance of the phase-sensitive gyroscopes. The designs with the shared proof mass have some mode-

coupling because excitation of one of the resonance modes leads to the deformation of the springs belonging to the other orthogonal mode.

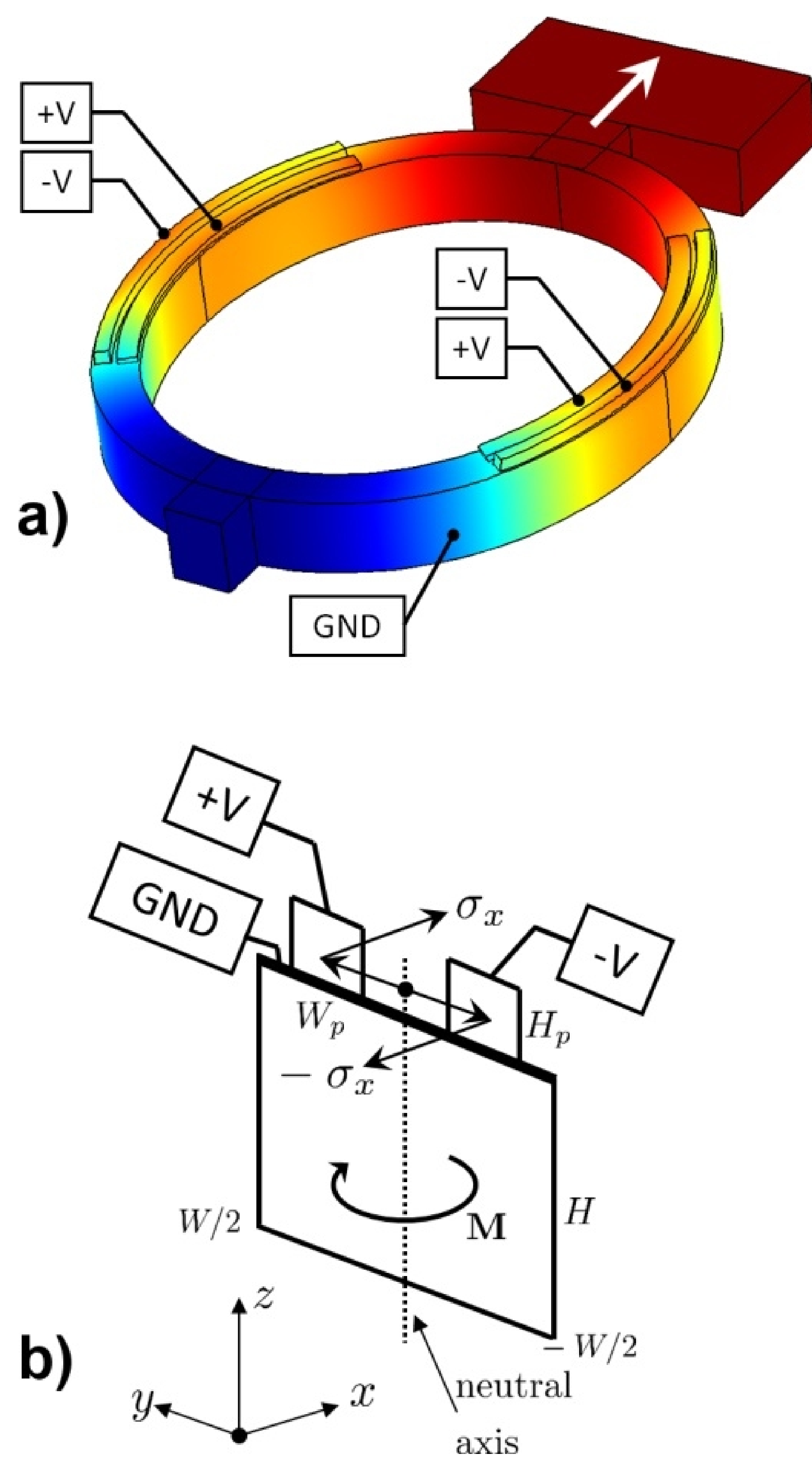


Figure 1. Thin-film piezoelectric in-plane actuation. a) FEM simulation of a linear resonator with thin piezoactuator layers on top of thick ring-shaped beam. By applying voltage of different polarities across the corresponding piezolayers, in-plane bending can be achieved. b) Stress $\pm\sigma_x$ in the corresponding piezolayers of width W_p and height H_p is a result of applied voltages, V . The bending moment M acting on the host beam of width W and height H can be obtained from integration of force couples due to $\pm\sigma_x$.

Figures 2a and 2b illustrate two designs of orbiting gyroscope with adequate mode-decoupling that are based on linear piezoactuated beams with annular decouplers and annular springs with piezoactuators directly on top of them, respectively. The ring-shaped flexures are suitable for supporting the orbiting motion and mode-decoupling due to their pronounced angle-dependent spring constant (Fig. 2c). Simulation results in Fig. 2c for a ring-shaped beam with 200 μm external radius and beamwidth of 20 μm

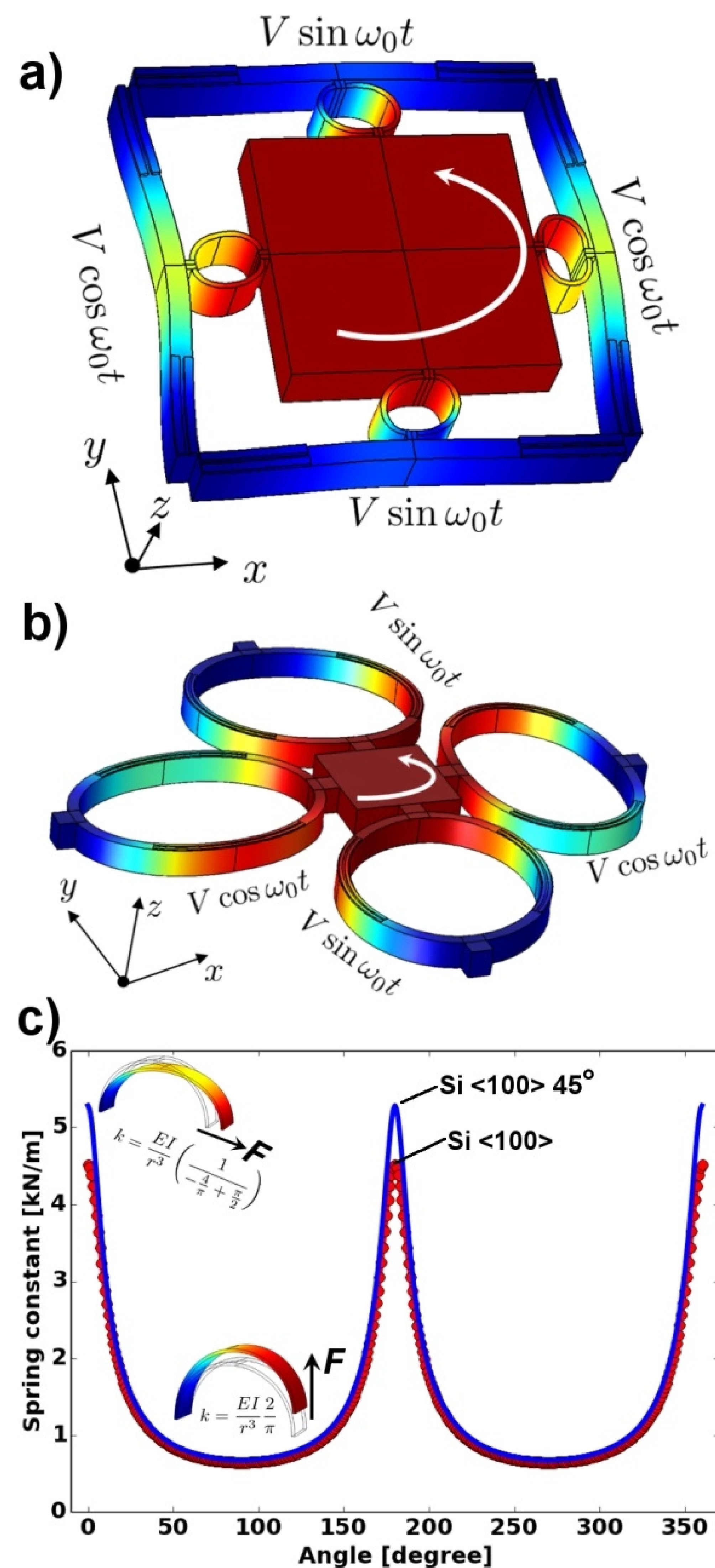


Figure 2. Simulated displacements of the proof mass due to voltages applied to the piezoactuators on (a) straight Si beams with ring-shaped decouplers, (b) annular, ring-shaped beams. Both (a) and (b) have orthogonal resonance modes along the X - and Y -axis. Driving both identical and orthogonal modes into resonance with harmonic voltages having 90 degrees phase difference results in orbiting of the proof mass. (c) Annular springs are suitable for decoupling the modes due to the angle-dependent spring constant that is considerably (factor of ~ 7 or ~ 7.8 for different orientations of the spring with respect to Si<100> crystal axis) more compliant in the “parasitic” (force F at 90°) compared to primary deformation (F at 0°).

indicate that the spring constant associated with the primary deformation (force F at 0° with

respect to the primary vibration direction resulting in stretch/compression of the springs) is a factor of ~ 7 larger than the spring constant associated with the “parasitic” deformation (force F at 90° with respect to the primary vibration direction resulting in “shear/roll” deformation of the spring). Due to the anisotropy of Si [2], the mode-coupling can be further decreased by increasing the ratio between primary and parasitic spring constants by re-orienting the springs in the wafer plane (Fig. 2c). The response of orbiting resonators with ring-shaped springs having actuators processed directly on top of them (Fig. 2b) to angular rates was analyzed in more detail using FEM simulations. Even though the mode-coupling of these designs is higher compared to the designs shown in Fig. 2a, the electromechanical coupling (i.e., transformation efficiency between mechanical and electrical signals) in these devices is higher making them more suitable for motion excitation and its sensing.

3. Simulation details and its verification

The performance of the resonators was simulated in a one-port drive-sense configuration (i.e., the same probe was used simultaneously for motion excitation and collection of the signal) in frequency domain by applying harmonic voltage V with appropriate phases to the corresponding piezolayers (Figures 1 and 2). The equations of motion were modified to account for the action of the Coriolis force due to the angular rate Ω on the proof mass (Eqs. 1). The response of the orbiting resonators to the angular rates was obtained from the phase-shift at the resonance frequency of the velocity of the proof mass (Fig. 3a) or the motional current through the piezolayers that was derived by integration of the current density from corresponding piezolayers’ boundaries. The following AlN material properties were assumed in the simulations: stiffness matrix components $C_{11}=360$, $C_{13}=C_{44}=120$ GPa; piezoelectric coupling matrix components $e_{31}=-0.58$, $e_{33}=1.55$ C m $^{-2}$; relative permittivity $\epsilon=9$. These material properties are comparable with the values for thin-film AlN in literature [3 and Refs. therein]. The analytical and derived from simulations sensitivity in terms of in terms of $^\circ/(\text{°/s})$, i.e., degrees of phase shift at resonance per $^\circ/\text{s}$ of angular rate for systems having identical X- and

Y-modes with various resonance frequencies and quality factors is shown in Figure 3b.

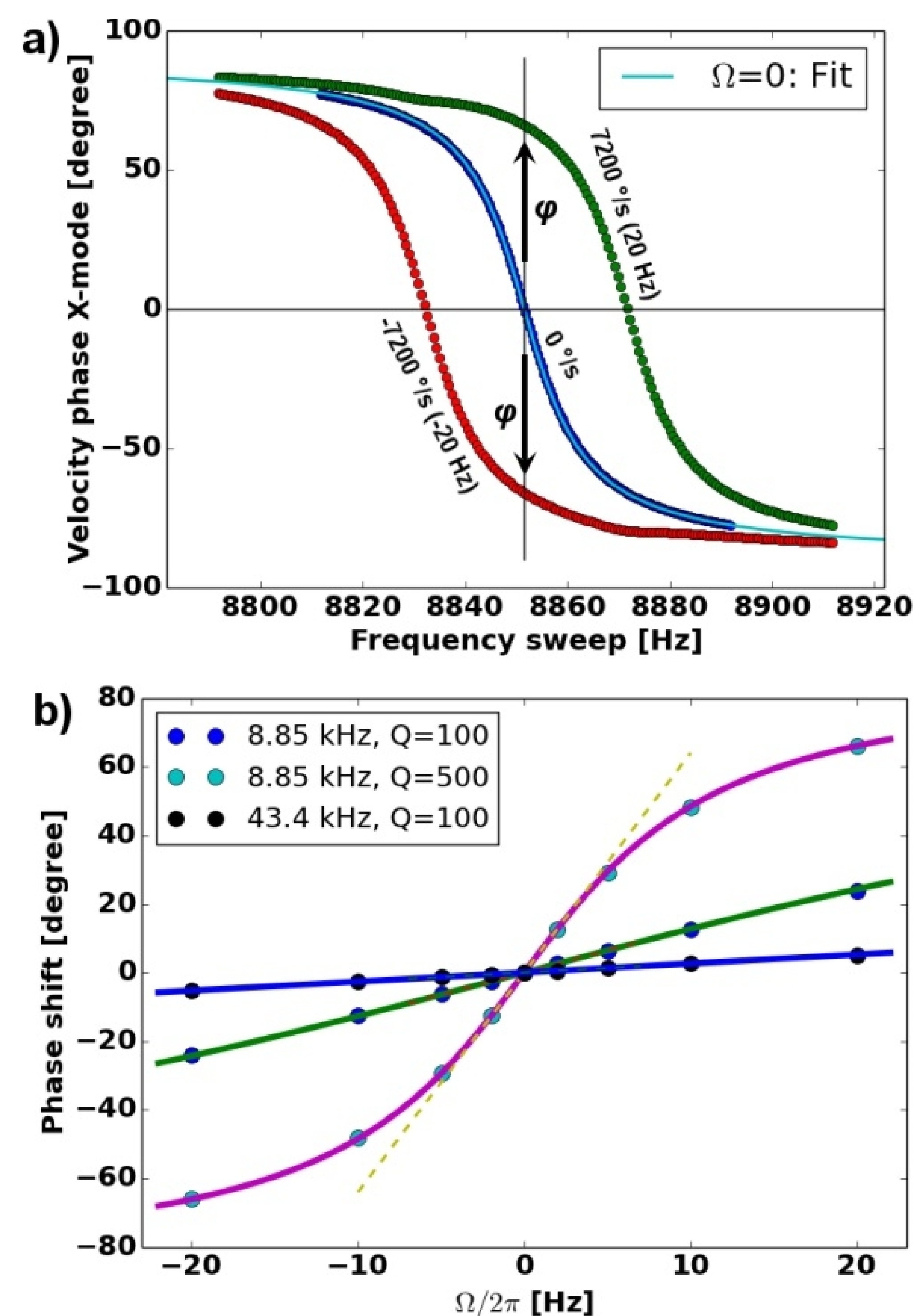


Figure 3. (a) Frequency domain simulations of the velocity phase (X-mode) at different angular rates (0 and ± 7200 °/s) of a device from Fig. 2b having resonance frequency of 8.85 kHz and Q-factor of 500. Angular rates induce phase-shifts ϕ at the resonance frequency. (b) Phase shifts for angular rates derived from simulation for systems with different resonance frequencies and Q-factors are compared with analytical values $\phi = \tan^{-1} \frac{-\omega_0^2}{2Q\Omega}$. The sensitivity to angular rates for a given system is linear in a certain range of angular rates (dashed line).

Systems having high Q-factors and low resonance frequencies tend to have higher sensitivity, however, they respond non-linearly to higher angular rates. For the device shown in Fig. 2b with springs radius 300 μm and beamwidth 14 μm having resonance frequency of 8.85 kHz with assumed Q-factors of 100 and 500 the simulated sensitivities in the range of ± 720 °/s are 3.5×10^{-3} $^\circ/(\text{°/s})$ and 17.5×10^{-3} $^\circ/(\text{°/s})$, respectively. For a similar device with springs radius 200 μm and beamwidth 22 μm having resonance frequency of 43.4 kHz with assumed Q-factors of 100 and 500 the simulated

sensitivities in the same range have better linearity but lower values of $0.71 \times 10^{-3} \text{ }^\circ/(\text{ }^\circ/\text{s})$ and $3.5 \times 10^{-3} \text{ }^\circ/(\text{ }^\circ/\text{s})$, respectively. In the experimental devices having quality factors $>20 \times 10^3$ in vacuum [4] the corresponding theoretical sensitivity can be considerably higher at $0.12 \text{ }^\circ/(\text{ }^\circ/\text{s})$, however, it is linear in the reduced range $\pm 360 \text{ }^\circ/\text{s}$ of angular rates.

The good agreement between the theoretical and simulated sensitivities of the orbiting piezogyroscopes validates the applicability of simulation to model more complex behaviours of the system not easily treatable analytically, e.g., response to the angular rates of the system having a mismatch between the resonance frequencies of the orthogonal modes, as well as for verifying various driving and read-out schemes.

4. Frequencies mismatch

Microfabrication imperfections and geometrical non-idealities in actual devices often lead to mismatch of the orthogonal modes' frequencies. The impact of the resonance frequency mismatch on the sensitivity of orbiting piezogyroscope was investigated in detail by simulating the device performance shown in Fig. 2b with springs' radius $200 \text{ } \mu\text{m}$ and beamwidth $14 \text{ } \mu\text{m}$ having ideally mode-matched resonance frequency of 43.4 kHz with assumed Q-factor of 500. To obtain the frequency mismatch, the springs of the Y-mode were uniformly broadened in the radial direction thus increasing their stiffness. The difficulty in matching the resonance frequencies is illustrated by the fact that even 7 nm overall broadening of the Y-mode's springs leads to the mismatch of 20 Hz . Figure 4 shows the frequency-dependent mechanical velocity and its phase response to the angular rates of a system with a large 500-Hz frequency mismatch (for illustrative purposes). The Coriolis force (Eqs. 1) cross-couples the modes giving rise to the energy flow between the split modes and appearance of secondary resonances at the frequencies of the corresponding orthogonal modes (Fig. 4a).

The effect of the mode-mismatch Δf ($\omega_y > \omega_x$) is summarized in Figure 5. For a given resonance frequency of the X-mode and Q-factor, the system has the highest sensitivity at $\Delta f = 0$, that decreases rapidly to zero as Δf increases. This decrease of the sensitivity is associated with the

reduced mechanical amplitude of the Y-mode when the system is driven into orbiting motion at the resonance frequency of the X-mode (Fig. 4a). Reduced Y-amplitude compared to the X-amplitudes implies that the proof mass orbits about an elliptical rather than circular path, resulting in the reduced phase-sensitivity of the gyroscope.

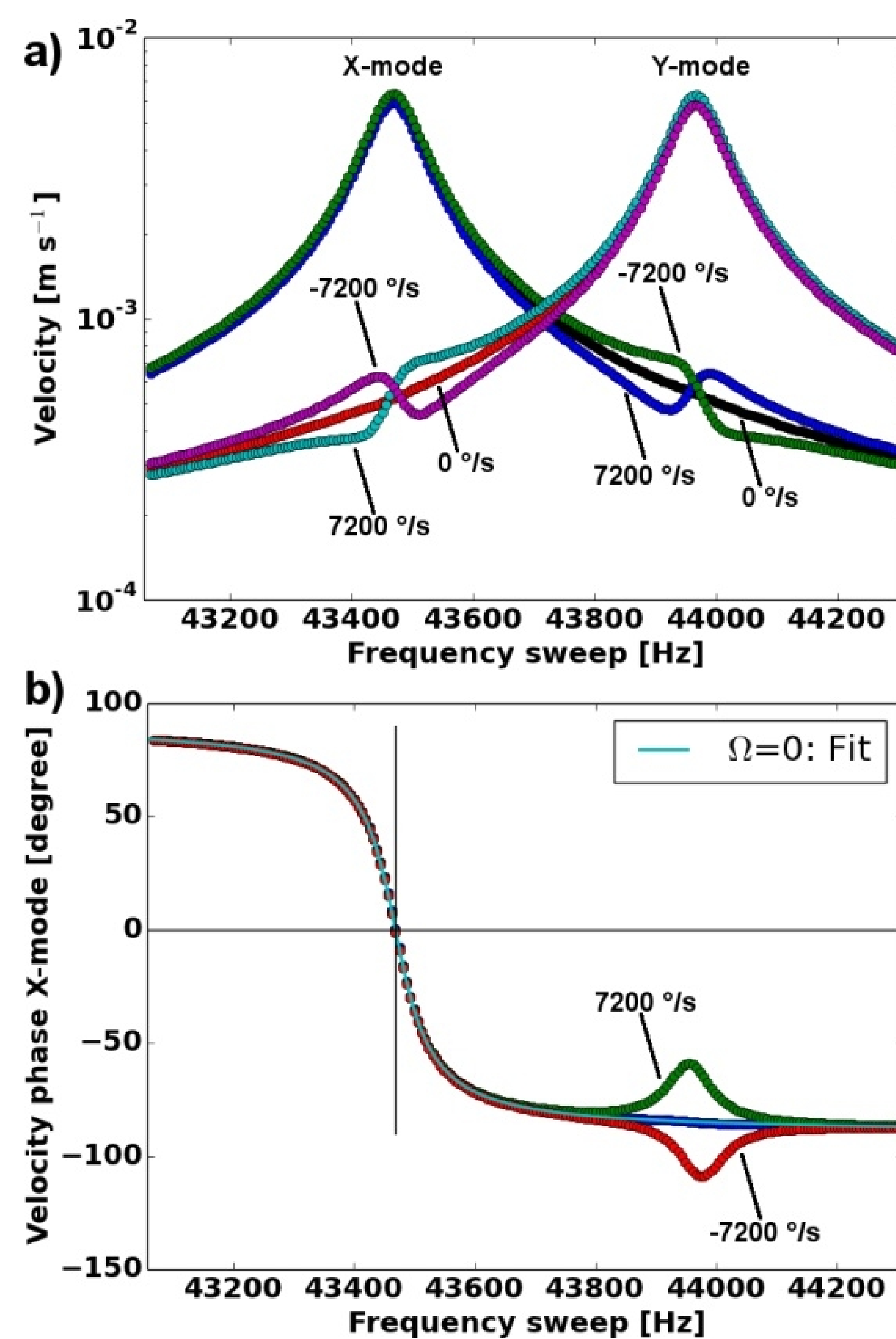


Figure 4. Frequency-domain simulation results of impact of 500-Hz frequency mismatch between the X- and Y-modes in a device from Fig. 2b for assumed Q-factor of 500. a) Velocity at different angular rates (0 and $\pm 7200 \text{ }^\circ/\text{s}$). b) Velocity phase (X-mode) at different angular rates.

The sensitivity, however, can be considerably improved even for systems having large Δf by matching the amplitudes of both modes. Figure 6a shows frequency-domain simulation of proof mass velocity per 1 V drive for 200-Hz frequency mismatch between the X- and Y-modes in a device from Fig. 2b for assumed Q-factor of 500. The amplitude of Y-mode at the resonance frequency of the X-mode is ~ 4.7 times lower compared with the X-amplitude such that the mass moves along an elliptical orbit. Driving the Y-mode at higher voltage (4.7 V) increases the Y-amplitude to the same level with the X-

amplitude thus enabling circular orbiting motion of the mass. Figures 6b and 6c compare the sensitivities for systems with and without amplitude-matching demonstrating considerably larger sensitivities in the amplitude-matched devices. Thus, even for a large mode-mismatch Δf of 200 Hz, the sensitivity can be improved by amplitude-matching by a factor of ~ 4.5 to the level of $0.72 \times 10^{-3} \text{ }^\circ/(\text{ }^\circ/\text{s})$, see Fig. 6c. Amplitude-matching is, therefore, a practical method to improve the sensitivity of devices with poor mode-match due to the, e.g., geometric non-idealities.

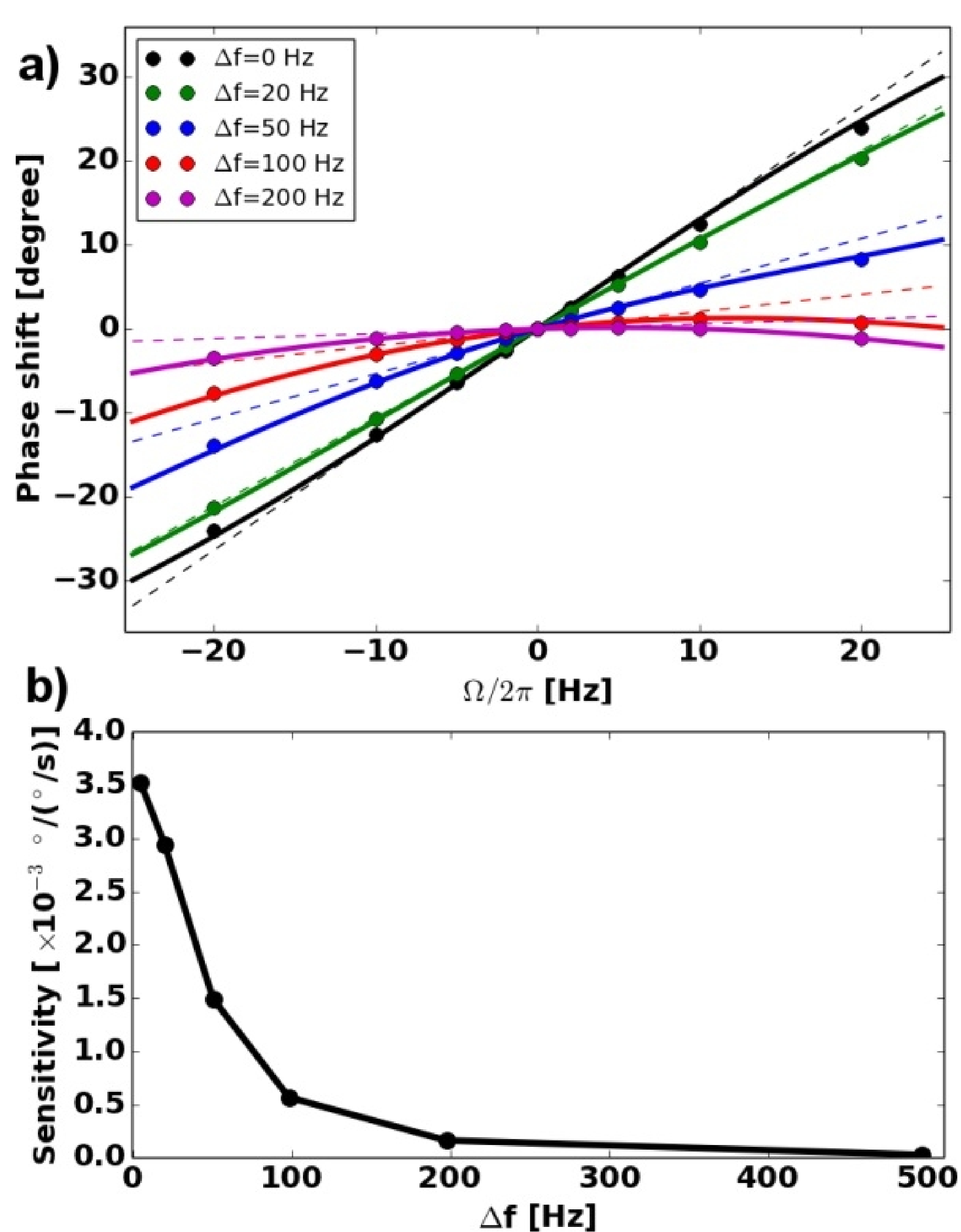


Figure 5. (a) Sensitivity of the X-mode to angular rates of orbiting piezogyroscopes with mismatch Δf in the orthogonal modes' resonance frequencies ($\omega_y > \omega_x$). Phase shifts for angular rates derived from simulation for a system from Fig. 2b with 43.4 kHz nominal resonance frequencies and Q-factor of 500 are compared with values obtained from solution of Eqs. 1 (solid lines). The sensitivity in the $\pm 720 \text{ }^\circ/\text{s}$ range is obtained from linear regression (dashed lines). (b) Summary of sensitivities for various Δf values.

5. Electromechanical performance

In practical devices, the amplitude information as well as phase-sensitivity to the angular rates cannot be obtained directly, but rather needs to be determined from the electrical

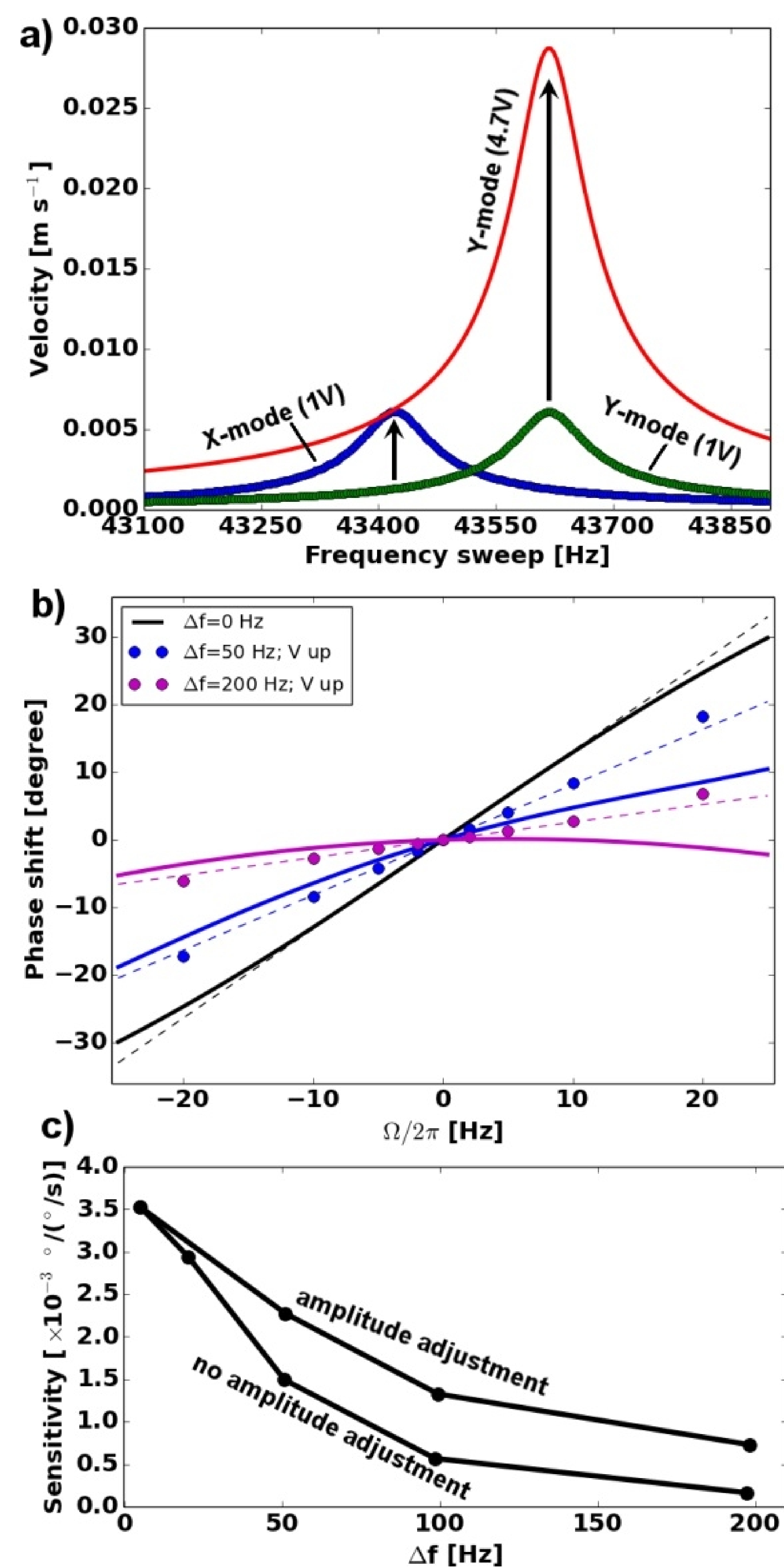


Figure 6. (a) Frequency-domain simulation of proof mass velocity per 1 V drive for 200-Hz frequency mismatch between the X- and Y-modes in a device from Fig. 2b for assumed Q-factor of 500. Driving the Y-mode at higher voltage (4.7 V) increases the Y-amplitude at the resonance frequency of the X-mode to the same level with the X-amplitude enabling circular orbiting motion of the mass. (b) Sensitivity of the X-mode to angular rates of orbiting piezogyroscopes with mismatch Δf in the orthogonal modes' resonance frequencies ($\omega_y > \omega_x$) and amplitude-matching by increased drive-voltage. Phase shifts for angular rates derived from simulation for a system from Fig. 2b with 43.4 kHz nominal resonance frequencies and Q-factor of 500 are compared with values obtained from solution of Eqs. 1 without amplitude-matching (solid lines). The sensitivity in the $\pm 720 \text{ }^\circ/\text{s}$ range was obtained from linear regression (dashed lines). (c) Summary of sensitivities for various Δf values with and without amplitude-matching.

response of the device. Figure 7a shows frequency response of the current via the piezoelectric films for both X- and Y-modes in one-port drive configuration (phases are with respect to the corresponding excitation voltages, $\Delta f=100$ Hz). Outside of the resonance, the signal is primarily due to the current flow through the capacitances formed by the piezoelectric layers (Fig. 7b, left).

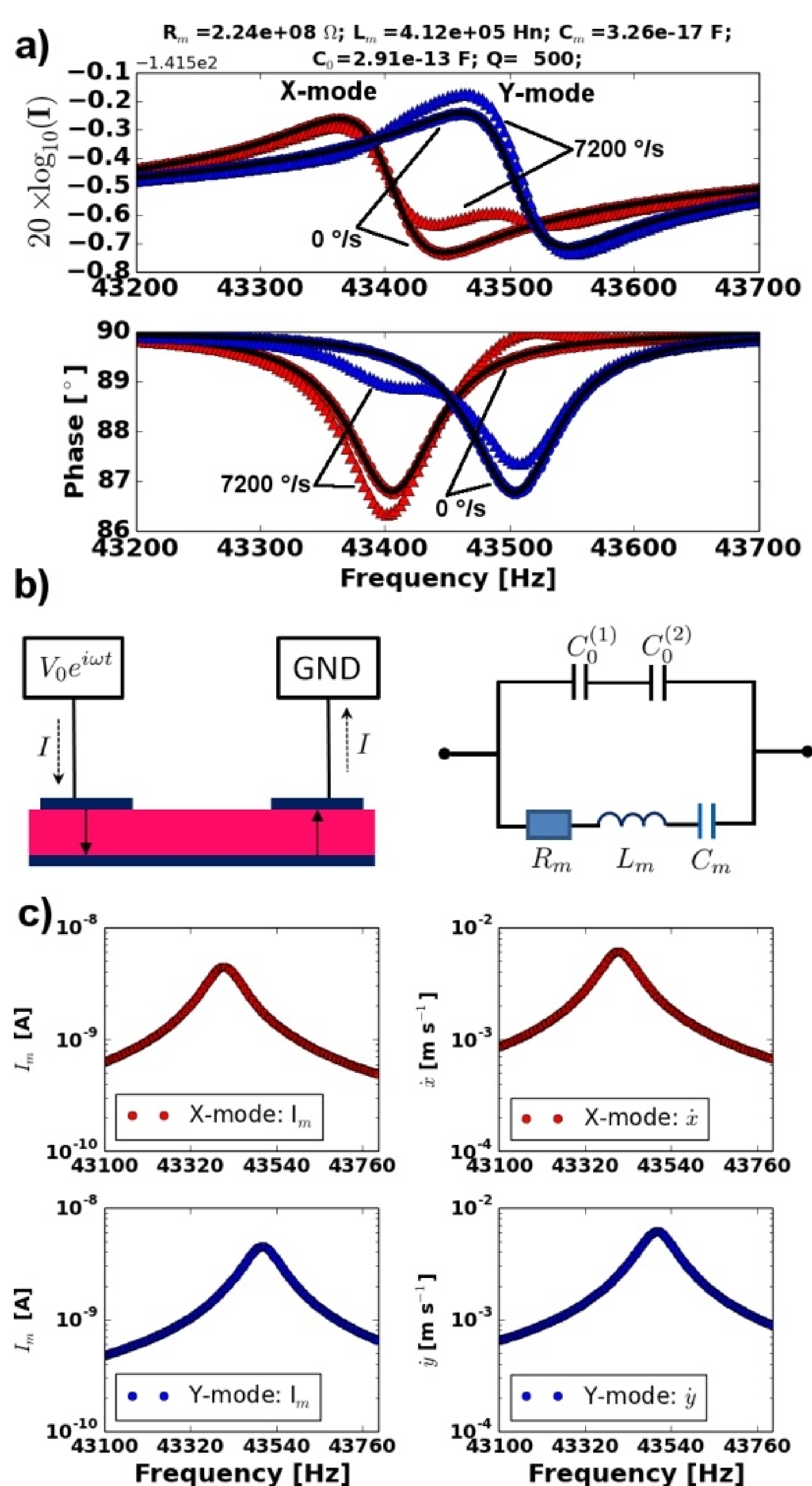


Figure 7. (a) Frequency response of the current through piezolayers for both X- and Y-modes separated by 100 Hz for 0 and ± 7200 °/s angular rates. Equivalent circuit parameters fits (black lines) are for 0 °/s with X-mode parameters shown in the title. (b) Schematic of one-port drive-read configuration with the equivalent circuit consisting of capacitances of the piezolayers ($C_0^{1,2}$) and mechanical $R_m L_m C_m$ branch. (c) Motional current I_m derived from the overall current by numerically removing contribution from the static capacitances is a velocity of the mass scaled by transduction factor η .

However, at the mechanical resonance the signal is increased due to the contribution of the motional current (due to the motion of the piezolayers). Such a system can be described in terms of equivalent circuit with static capacitances $C_0^{1,2}$ of the piezolayers connected in parallel with the mechanical $R_m L_m C_m$ branch (Fig. 7, right). The mechanical performance of the resonator can be indirectly evaluated from its electrical performance using the equivalent circuit parameters. The parameters $R_m L_m C_m$ (motional resistance, inductance and capacitance) are scaled damping coefficient, mass and spring constant of the resonator, respectively. Thus, the effective mass load, m , of the resonator and the motional inductance are related as $L_m = m/\eta^2$, where the scaling coefficient η is the transduction factor, e.g., the actuation force generated per applied 1V of AC-voltage, such that $F_0 = \eta V$. In the studied system (Fig. 2b), the proof mass m can typically be derived from its geometrical dimensions (2.13×10^{-7} kg) and used to evaluate η ($0.72 \mu\text{N/V}$) from the fitted value of L_m (0.412 Mh, Fig. 7a). On the other hand, the motional current flowing through the mechanical $R_m L_m C_m$ branch can be written as $I_m = \eta \dot{x}$, where \dot{x} is the mechanical velocity of the resonator. The scaling coefficient between the electrical and mechanical domain can, therefore, be also derived from the ratio between the motional current and the proof mass velocity.

The overall current through the resonator can be described as $I = V/Z = VY$, where V is the driving voltage, Z and Y are complex impedance and admittance, respectively. The total admittance of the circuit shown in Fig. 7b is

$$Y_{tot} = i\omega C_0 + \frac{1}{R_m + i\omega L_m + \frac{1}{i\omega C_m}} \quad (2)$$

The motional current I_m (Fig. 7c, left) can be estimated by subtracting the current $i\omega C_0$ through the static capacitors from the overall current (Fig. 7a) using C_0 values obtained from the equivalent circuit parameters fit. It can be shown that I_m (Fig. 7c, left) and the proof mass velocity amplitude (Fig. 7c, right) are proportional within a scale factor η of 0.73×10^{-6} . This value of η , derived directly from the velocity and motional current amplitude, is in good agreement ($<2\%$) with the value obtain

indirectly from the equivalent circuit parameters and mass of the system. The amplitude-matching can, therefore, be reliably performed by using the electromechanical response of the systems where amplitude measurements are not available. Furthermore, using the $R_m L_m C_m - C_0$ circuit-fits the amplitude-matching of the modes can be performed even in systems that, due to the geometric imperfections, have in addition to the frequency-mismatch also mismatch of the Q-factors or transduction factors η . Since the measurable I_m is the scaled mechanical velocity of the resonator, the phase-shift of the motional current can be used for detection of the angular rates. Thus, even in the simple one-port drive-sense configuration the devices can perform as phase-sensitive orbiting gyroscopes. The gyroscope performance can be further optimized and other more complex and potentially more sensitive drive-sense configurations can be verified by using the modelling of devices.

8. Conclusions

The feasibility of phase-sensitive detection of angular rates using orbiting resonators suspended by thick annular springs with thin-film aluminium nitride piezoactuators on top of the springs was investigated. The orbiting motion of the proof mass can be achieved by driving identical and orthogonal modes of a mass-on-springs system into resonance with harmonic excitations having $\pi/2$ rad phase difference. External rotation of the system modifies its mechanical response manifested in a phase-shift at resonance. The performance of the piezoresonators was simulated in a one-port drive-sense configuration in frequency domain and accounting for the action of the Coriolis force on the proof mass. The sensitivities in terms of phase shift at resonance of up to $17.5 \times 10^{-3} \text{ }^\circ/(\text{ }^\circ/\text{s})$ to the angular rates in the $\pm 720 \text{ }^\circ/\text{s}$ range were obtained from the phase-shifts at the resonance frequency of the motional current for a studied system with a Q-factor of 500 and resonance frequency of 8.85 kHz. The sensitivities are considerably higher in systems with higher Q-factors at the expense of the range of the angular rates in which the sensitivity is linear. The theoretical angular-rate-induced phase shifts and those derived from simulations and are in good agreement for simple systems with identical orthogonal modes, hence verifying

the model. The simulations were further verified for more complex systems with orthogonal modes having different resonance modes. Due to the frequency mismatch between the modes, the sensitivity of the system is reduced. By driving one of the modes with a higher voltage such that its vibrational amplitude is increased to the same level with the other mode's resonance amplitude, the sensitivity can be considerably increased. Using simulations, the electrical response of the system can be modeled, its equivalent circuit parameters can be obtained, performance optimized and various potentially more sensitive drive-sense schemes verified.

9. References

1. M. Dalal, A.N. Shirazi, W.K. Sung, G. Casinovi, F. Ayazi, Novel read-out scheme for MEMS vibratory gyroscopes based on signal phase shifts, *Solid-State Sensors, Actuators and Microsystems Worksop*, 328-331 (2012)
2. D. Kwak, J. Kim, S. Park, H. Ko and D.-I. Cho, Article title, Why is (111) Silicon a better mechanical material for MEMS, from http://www-mtl.mit.edu/researchgroups/mems-salon/sriram_Si-111-better.pdf
3. A.V. Sotnikov, H. Schmidt, M. Weihnacht, E.P. Smirnova, T.Yu. Chemekova, Yu.N. Makarov, Elastic and piezoelectric properties of AlN and LiAlO₂ single crystals, *IEEE Transaction on ultrasonic, ferroelectric and frequency control*, **57**, 808-811 (2010)
4. S. Gorelick, J.R. Dekker, B. Guo, H. Rimminen, Piezoelectrically actuated resonators on ring-shaped suspensions for applications in MEMS phase-sensitive gyroscope, *Procedia Engineering* (2014) submitted.

10. Acknowledgements

This contribution was developed within the scope of the CATHRENE project EM4EM (CA 310; Electromagnetic Reliability of Electronic Systems for Electro Mobility) which is funded by TEKES (Finnish Funding Agency for Technology and Innovation) by funding decision 40471/11. The responsibility for this publication is held by authors only.